applied sciences

MDPI

*Article*

# Incident Angle Dependence of the Waveform of the Polarization-Sensitive Photoresponse in CuSe/Se Thin Film

**Arseniy E. Fateev, Tatyana N. Mogileva, Vladimir Ya. Kogai, Konstantin G. Mikheev and Gennady M. Mikheev ***

Institute of Mechanics, Udmurt Federal Research Center, Ural Branch of the Russian Academy of Sciences, Tatyana Baramzinoy Street, 34, 426067 Izhevsk, Russia; a.e.fateev@mail.ru (A.E.F.); mogileva@udman.ru (T.N.M.); vkogai@udman.ru (V.Y.K.); k.g.mikheev@udman.ru (K.G.M.)

* Correspondence: mikheev@udman.ru; Tel.: +7-3412-21-66-11

**Abstract:** The results of studying the waveforms of longitudinal and transverse photocurrent pulses generated in thin, semitransparent CuSe/Se films as a function of the angle of incidence ($\alpha$) of a femtosecond laser beam at linear and circular polarizations are presented. It has been established that the durations of unipolar longitudinal photocurrent pulses at linear and circular polarizations of laser pumping do not depend on the angle $\alpha$. It is shown that the evolution of the temporal profile of the helicity-sensitive transverse photocurrent with a change in $\alpha$ strongly depends on polarization. At linear polarization, the shape of the unipolar pulses remains virtually constant; however, at circular polarization, the generation of unipolar and bipolar pulses is possible, with the waveforms strongly depending on the angle $\alpha$. The influence of the incidence angle on the waveforms of transverse photocurrent pulses is explained by the transformation of linear and circular polarization into an elliptical upon the refraction of light at the air/semitransparent film interface and by the interplay of photocurrents arising due to linear and circular surface photogalvanic effects in the film. The presented findings can be utilized to develop polarization and incidence angle-sensitive photovoltaic devices.

**Keywords:** circular photocurrent; polarization; helicity; bipolar photovoltage; waveforms; femtosecond excitation; surface photogalvanic effect; thin films



**Citation:** Fateev, A.E.; Mogileva, T.N.; Kogai, V.Y.; Mikheev, K.G.; Mikheev, G.M. Incident Angle Dependence of the Waveform of the Polarization-Sensitive Photoresponse in CuSe/Se Thin Film. *Appl. Sci.* **2022**, *12*, 6869. https://doi.org/10.3390/app12146869

Academic Editor: Alejandro Pérez-Rodróhiez

Received: 12 May 2022
Accepted: 5 July 2022
Published: 7 July 2022



## 1. Introduction

One of the interesting features of the interaction of polarized light [1–3] with semiconductors and metals is the generation of a polarization-sensitive photocurrent (PSPC) that depends on the polarization of the incident radiation according to harmonic laws [4–9]. There are longitudinal and transverse PSPCs at the oblique incidence of light on the surface of a material in which the currents flow along and perpendicular to the plane of incidence, respectively [10]. The transverse PSPC can be a combination of circular photocurrents (CPC) and linear photocurrents (LPC). The CPC depends on the direction of rotation of the electric field vector (the sign of circular polarization) of the incident radiation, while the LPC does not [11–14]. It is of interest to study the laws governing the PSPC in various media in terms of excitation of spin-polarized electrons [15,16], for the creation and development of optospintronic devices [17], laser polarization analyzers [18–20], photodiodes with high spatial resolution [21], as well as for photosensors intended for the direct recording of the polarization state of circularly polarized light [22–25]. The mechanisms of the PSPC generation include the photogalvanic effect (PGE) [26–28], the circular photogalvanic effect (CPGE) [11,29–34], the photon drag effect (PDE) [5,10,35–38], and the surface photogalvanic effect (SPGE) [5,39,40]. All of the aforementioned effects are nonlinear optical phenomena. It should be noted that the PDE and SPGE, as well as some other nonlinear optical phenomena [41,42] can be observed in any media, regardless of the type of symmetry of the medium [35]. The PDE and SPGE photocurrent pulses excited by pulsed laser pumping are usually unipolar (see, for example, [14,43–46]). The dependence of CPC and LPC excited in film and 2D structures due to the PDE and SPGE on the beam incidence angle $\alpha$ is described by an odd function [36,37,39,46–48]. Therefore, under pulsed laser pumping, the LPC and CPC unipolar pulses change their polarity when the sign of the incidence angle changes. With the simultaneous occurrence of longitudinal PDE and SPGE, due to their interplay, it is possible to generate bipolar PSPC pulses consisting of front and tail parts of opposite polarity, which change their polarities when the sign of the angle of incidence changes [40]. It was shown in our most recent work [48] that, at a given angle of incidence, the interference of the CPC and LPC generated due to the SPGE in a CuSe/Se nanocomposite film also leads to the generation of bipolar photocurrent pulses. The temporal profiles of those pulses strongly depend on the polarization ellipse of the incident femtosecond laser beam. However, despite the large number of articles on the topic of PSPC generation in various film materials (see, for example, [33,38,49–52]), studies of the influence of the incidence angle on the waveforms of photocurrent pulses arising due to the PDE and SPGE (and also CPGE) under pulsed laser pumping have not been carried out yet.

In this work, using the study of the SPGE in a CuSe/Se semitransparent thin film under femtosecond laser excitation as an example, it is shown for the first time that the waveforms of the PSPC pulses can strongly depend on the angle of incidence. In particular, it has been shown that with circularly polarized pulsed pumping and a fixed sign of the incidence angle, unipolar transverse photocurrent pulses of opposite polarity are generated at small and large angles of incidence, and bipolar pulses are excited in the intermediate range of incident angles, smoothly transforming into unipolar pulses of opposite polarity at the boundaries of this interval. The results obtained are explained by the change in the state of polarization in the refracted beam and by the interference of the LPC and CPC that arises in the subsurface layer of the semiconducting medium under study.

## 2. Materials and Methods

Thin CuSe/Se films with a thickness of 130 nm and dimensions of 15 × 35 mm were synthesized on a glass substrate by successive vacuum thermal deposition of Se and Cu, according to the procedure described in one of our previous publications [14]. To stabilize the residual Se [53,54], the synthesized film structure was annealed at a temperature of 140 °C for 30 min. As a result, the selenium from an unstable amorphous phase was transformed into a stable polycrystalline trigonal selenium (*t*-Se). It should be noted that currently there are some other methods of film copper selenides structure synthesis that have also been developed [55–60].

The phase composition of the films was studied at room temperature on a Bruker D2 PHASER diffractometer. We used CuK$\alpha$ radiation ($\lambda$ = 0.154 nm). Using the DIFFRAC.EVA universal program, the diffraction curves were smoothed and the background due to X-ray scattering on a glass substrate was subtracted. To study the phase composition of the films, we additionally used a HORIBA HR800 Raman spectrometer with laser excitation at 632.8 nm at the radiation intensity of 14 kW/cm$^2$. Sample surface images were taken using a scanning electron microscope (SEM) (Thermo Fisher Scientific Quattro S, Brno-Černovice, Czech Republic). The elemental composition of the synthesized films was determined using an energy-dispersive microanalyzer based on an EDAX "Octane Elect Plus EDS System" spectrometer built into the SEM. The optical transmittance spectra of the films were recorded using a two-beam spectrophotometer (PerkinElmer Lambda 650, Shelton, WA, USA). The film thickness was measured using a stylus profilometer. The refractive index $n$ and the extinction $\kappa$ of the film were determined using an ellipsometer.

The X-ray diffraction pattern (see Figure S1, Supporting Information) and the Raman spectrum (see Figure S2, Supporting Information) demonstrate that the film has two phases and consists of CuSe and *t*-Se. The mass percentages of CuSe and *t*-Se in the synthesized film are 33.3 and 66.7 wt.%, respectively. The film surface consists of a number of flat petallike structures, which are CuSe crystallites predominantly oriented in radial directions from their centers (see Figure S3, Supporting Information). The centers of these structures are located at distances of about 15–30 μm from each other. The film is semitransparent in the visible wavelength range (see Figure S4, Supporting Information). The optical transmittance, refractive index *n*, and extinction coefficient κ at 795 nm are 27.6%, 1.64, and 2.14, respectively. The synthesized film is electrically conductive with a sheet resistance of 39 Ω/□, which is orders of magnitude lower than the corresponding value of many known thin-film semiconductor structures (see, for example, [61,62]). It should be added that the sheet resistance of CuSe thin films with thicknesses from 50 to 500 nm synthesized by the chemical bath method varies between 23–50 Ω/□ [63]. Meanwhile, the sheet resistance of 280 nm thick bismuth selenide ($Bi_2Se_3$) film obtained by the same method immediately after synthesis is $10^{12}$ Ω/□, and after its annealing in air or in the nitrogen medium, the sheet resistance decreases to $3.6 \times 10^3$ Ω/□ [64].

To measure the laser-induced photocurrent (photovoltage), two film gold electrodes A and B were deposited on opposite short sides of the synthesized film by vacuum thermal deposition. The film under study was placed on a special goniometric device, which made it possible to smoothly change its spatial orientation relative to the incident laser beam. The surface of the film remaining after depositing the electrodes was sufficient to study the generation of photocurrent under the action of a narrow laser beam 1.5 mm in diameter in a wide range of incidence angles.

The photocurrent pulses in a CuSe/*t*-Se nanocomposite film were excited by pulses of a Ti:S femtosecond laser at a wavelength of 795 nm (pulse duration 120 fs, pulse repetition rate 1 kHz) at an oblique incidence of radiation on the film. All the experiments were carried out at laser pulse energy $E_{in}$ = 100 μJ. The polarization of the radiation incident on the film was controlled using half-wave and quarter-wave plates. The photocurrent pulses were registered and recorded using a digital oscilloscope with a bandwidth of 400 MHz and a rise time of 875 ps with averaging over multiple exciting laser pulses. The input impedance of the oscilloscope was $R_{in}$ = 50 Ω. In the experiments, the extreme values of the pulses of the longitudinal and transverse photocurrents $j_x$ and $j_y$, respectively, were recorded, determined by the formulas $j_x = U_x/R_{in}$ and $j_y = U_y/R_{in}$, where $U_x$ and $U_y$ are the extreme values of the voltage pulses at the experimental geometries when the measuring electrodes were placed perpendicular and parallel to the plane of incidence, respectively. Since $U_x$ and $U_y$ depend linearly on $E_{in}$ [65], it was convenient to introduce the conversion coefficients $\eta_x = j_x/E_{in}$ and $\eta_y = j_y/E_{in}$, which characterize the efficiency of converting light into longitudinal and transverse photocurrents, respectively. It should be noted that when studying the waveforms of the photocurrent pulses, we subtracted the time-varying background signal due to noticeable electrical interference coming from the power supply unit of the femtosecond laser.

## 3. Results and Discussion

Figure 1a shows the dependences of the coefficients of light conversion into longitudinal photocurrent $\eta_x$ on the angle of incidence α for linear and circular polarizations, measured according to the sketch of experimental arrangements presented in the upper frame. It can be seen that the photocurrent is absent at normal incidence of the radiation on the film (α = 0). The photocurrent changes polarity when the sign of the angle of incidence changes, increases in absolute value with an increase in the modulus of α, takes its extreme values at angles $|\alpha| \approx 66$–$68°$, and disappears at a grazing incidence of radiation on the film. Thus, the longitudinal photocurrent for linear and circular polarizations is described by an odd function of the angle α:

$$\eta_x(\alpha) = -\eta_x(-\alpha). \quad (1)$$

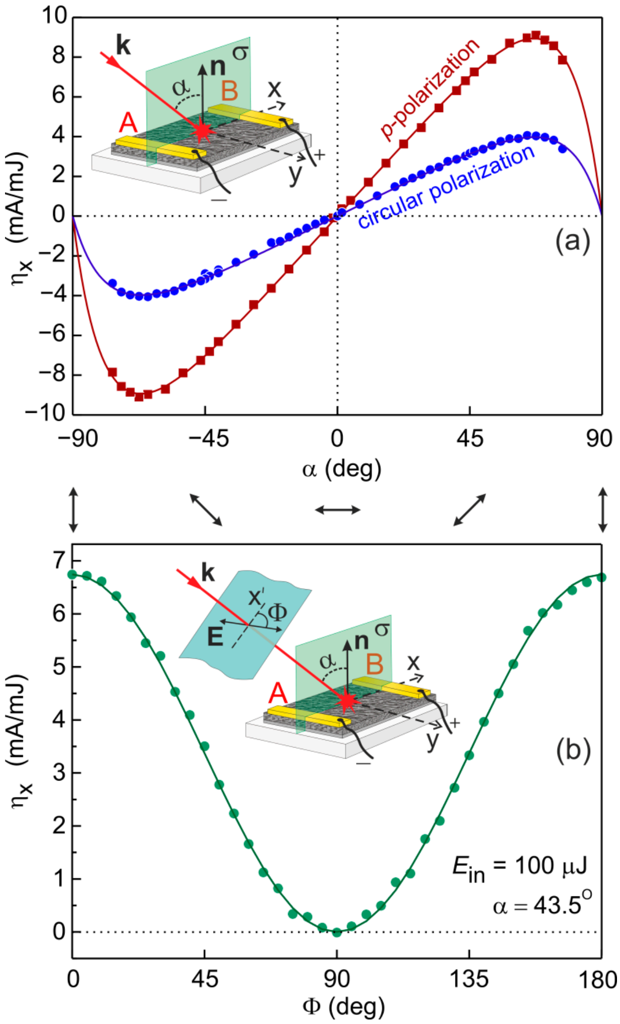


**Figure 1.** The light to longitudinal photocurrent conversion coefficient $\eta_x$ as a function of (**a**) the light incidence angle $\alpha$ on the film at linear (*p*-polarization) and circular polarizations (points denote experimental results, curves denote fitting with $\eta_x = 35.37\sin 2\alpha/(1.76\cos\alpha + 1)^2$ and $\eta_x = 15.68\sin 2\alpha/(1.75\cos\alpha + 1)^2$ for linear and circular polarization, respectively) and (**b**) the azimuth of the polarization plane $\Phi$ at $\alpha$ = 43.5° (dots denote experimental results, curve denotes fitting with $\eta_x(\Phi) = 6.7\cos^2\Phi$; orientations of the polarization plane are shown at the top). The insets show the sketches of the experimental setups: **k** and **E** are the wave vector and the electric field vector of the incident radiation, respectively; $\sigma$ is the plane of incidence; $\alpha$ is an angle of incidence; **n** is the normal to the film surface; **A** and **B** are the measuring electrodes; x, y are the axes of the rectangular coordinate system; the x and x′ axes lie in the $\sigma$ plane (x′ $\perp$ **k**, the x axis is perpendicular to the electrodes **A** and **B**); $\Phi$ is the angle between the x′ and **E**.

With linear polarization, the dependence of $\eta_x$ on the polarization azimuth $\Phi$ (the angle between the plane of polarization and the radiation incidence plane on the film $\sigma$) at a fixed $\alpha$ is described by an even function:

$$\eta_x(\alpha, \Phi) = \eta_x(\alpha, \Phi = 0)\cos^2, \tag{2}$$

where $\eta_x(\alpha, \Phi = 0)$ is the conversion coefficient at a given $\alpha$ and $\Phi$ = 0. It should be noted that $\Phi$ = 0 corresponds to *p*-polarized radiation. All this is clearly seen from the dependence $\eta_x(\Phi) = \eta_x(\alpha, \Phi = 0)\cos^2\Phi$ obtained at $\alpha$ = 43.5°, where $\eta_x(\alpha, \Phi = 0) = 6.7$ mA/mJ (see Figure 1b). From Equation (2) it follows that $\eta_x(\alpha = 43.5°, \Phi = 90°) = 0$, i.e., no photocurrent is generated at *s*-polarization. Experiments have shown that this equation is valid for any $\alpha$. Figure 2a shows the dependence of the conversion coefficient of light into transverse photocurrent $\eta_y$ on the angle of incidence $\alpha$ for linearly polarized radiation at polarization azimuth $\Phi = -45°$, obtained using the experimental setup shown in the upper inset to this figure. It can be seen that, similarly to the angular dependence of the longitudinal photocurrent, the experimental dependence $\eta_y(\alpha)$ is described by an odd function, i.e.:

$$\eta_y(\alpha) = -\eta_y(-\alpha). \quad (3)$$

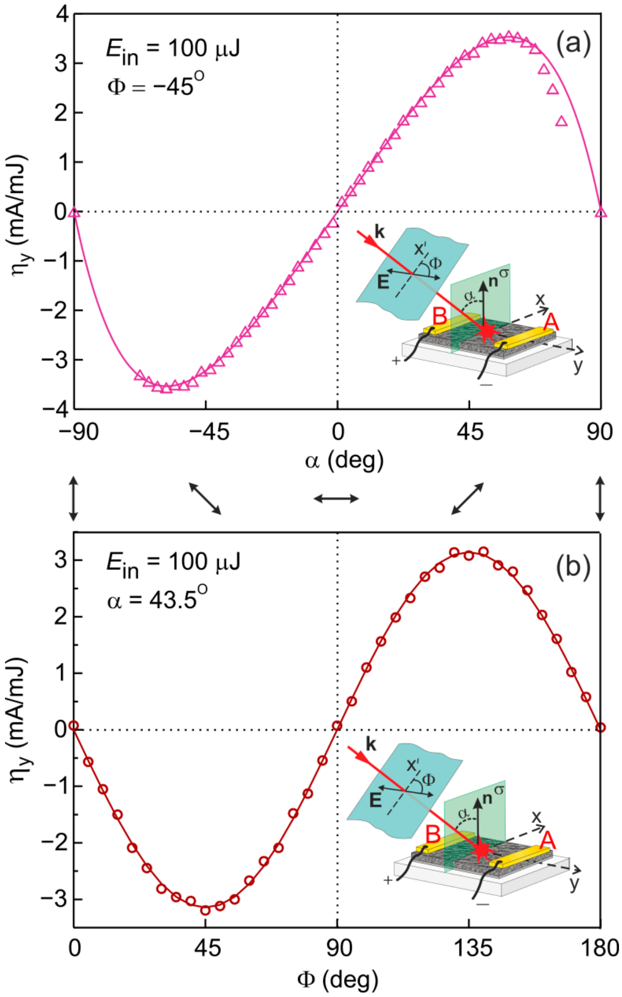


**Figure 2.** The light to transverse photocurrent conversion coefficient $\eta_y$ as a function of (**a**) the incidence angle $\alpha$ at the polarization azimuth $\Phi = -45°$ (triangles correspond to the experimental data while the solid line represents the result of the fitting with equation $\eta_y = 8.37 \sin 2\alpha/(0.87 \cos \alpha + 1)^2$) and (**b**) the polarization azimuth $\Phi$ at $\alpha = 43.5°$ (circles denote experimental data, the solid curve represents the fitting with the equation $\eta_y = -3.1 \sin 2\,\Phi$; the orientations of the plane of polarization of the incident radiation are shown at the top). The insets show the sketches of the experimental setups.

Meanwhile, the measured dependence of the transverse photocurrent on the polarization azimuth $\Phi$ at a fixed $\alpha = 43.5°$ (see Figure 2b) is approximated by an odd function:

$$\eta_y(\alpha = 43.5°, \Phi) = \eta_y(\alpha = 43.5°, \Phi = 45°) \sin 2\Phi, \quad (4)$$

where $\eta_y(\alpha = 43.5°, \Phi = 45°)$ is the conversion coefficient of light into transverse photocurrent at $\alpha = 43.5°$ and $\Phi = 45°$.

The set of angular and polarization dependences described by Equations (1)–(4) shown in Figures 1 and 2 indicates that the generation of photocurrent in the studied CuSe/*t*-Se thin films occurs according to the SPGE mechanism [5,39,40,65].

Figure 3a shows the unipolar pulse waveforms of the longitudinal photovoltage (measured in the geometry of the experiment when the measuring electrodes are oriented perpendicular to the plane of incidence), normalized to their extreme values at *p*-polarization of the incident radiation at $\alpha = \pm 45°$ and $\alpha = \pm 78°$. It follows that when the sign of the incidence angle is changed, the pulses are inverted, which is in agreement with Equation (1). It can also be seen that the waveforms of the pulses are virtually independent of the angle of incidence. This is evidenced by the dependence curve of the pulse duration $\tau$ (FWHM) on $\alpha$, presented in the inset to Figure 3a. Similar patterns were obtained when the longitudinal photovoltage was excited by circularly polarized radiation pulses (see Figure 3b). Thus, the waveforms of the longitudinal photovoltage pulses in the films under study for linear and circular polarizations are virtually independent from the angle of incidence.

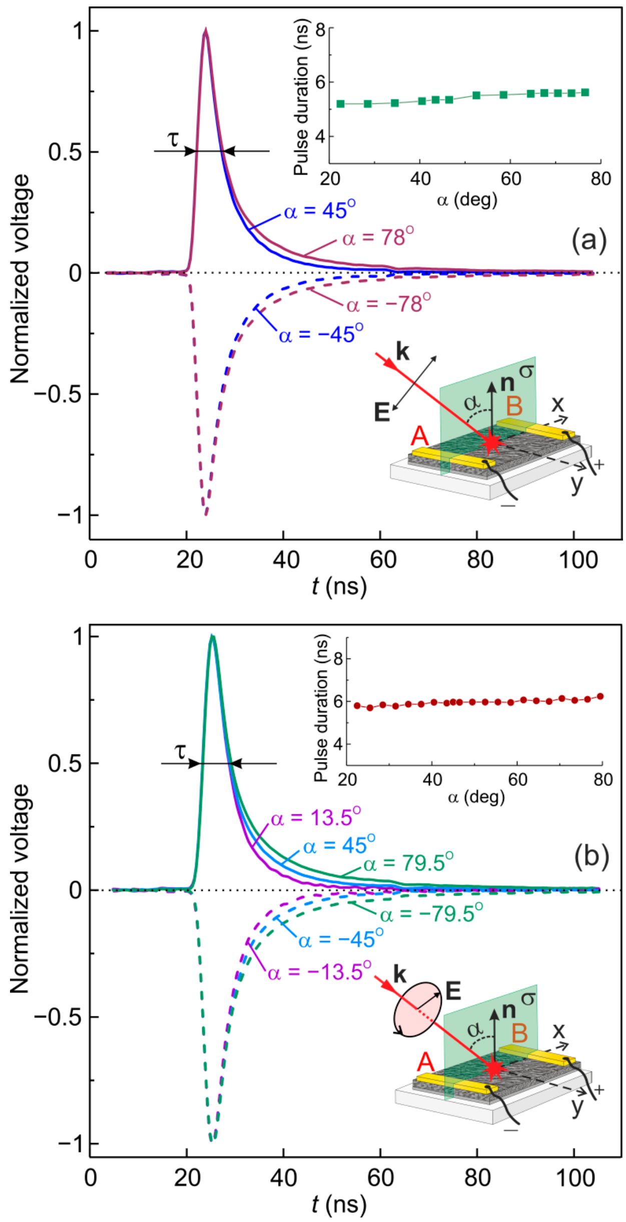


**Figure 3.** The waveforms of the longitudinal photovoltage pulses normalized to their extreme values at (**a**) linear polarization ($\Phi = 0$, *p*-polarization) and (**b**) circular polarization recorded at positive (solid lines) and negative (dashed lines) incidence angles $\alpha$. The upper insets show the corresponding dependences of the recorded pulse durations $\tau$ on the angle of incidence. The bottom insets show the sketches of the experimental setups.

The waveforms of the transverse photovoltage pulses recorded at linear polarization ($\Phi = -45°$) and normalized to their extreme values at different $\alpha$ are shown in Figure 4. It can be seen that the waveforms of these pulses weakly depend on $\alpha$. This is evidenced by the dependence of the pulse duration on the incidence angle, shown in the inset in the same figure.

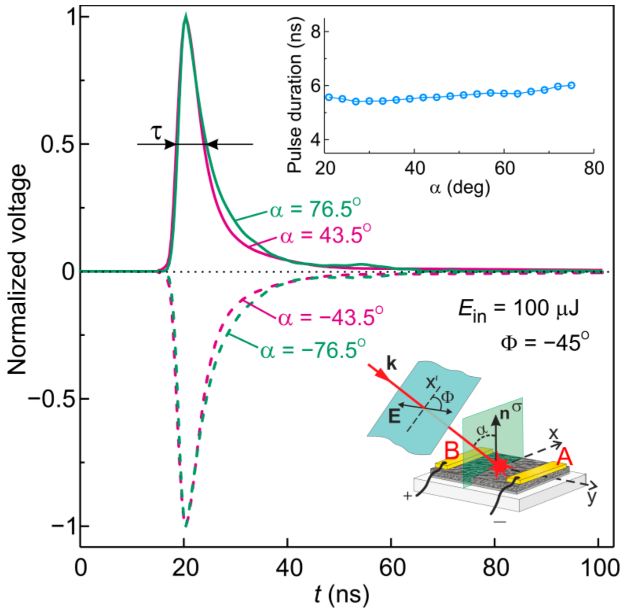


**Figure 4.** The waveforms of the transverse photovoltage pulses normalized to their extreme values at linear polarization ($\Phi = -45°$), recorded at positive (solid lines) and negative (dashed lines) angles of incidence $\alpha$. The upper inset shows the dependence of the recorded pulses duration $\tau$ on the angle of incidence. The bottom inset shows the sketch of the experimental setup.

Figure 5 shows the waveforms of the transverse photovoltage pulses recorded for the right-hand circularly polarized laser beam at various angles of incidence. The pulses are normalized to their extreme values. It can be seen that at $0 < \alpha < 58.5°$, positive pulses are generated, the duration of which gradually increases with increasing $\alpha$. In the range of angles $\alpha$ approximately $58.5 \leq \alpha \leq 76.5°$ bipolar pulses are excited. Figure 5 shows that at $\alpha = 58.5°$, a small negative pulse appears on the leading edge of the positive pulse. The amplitude of the front negative pulse increases with increasing the angle of incidence, while the amplitude of the positive tail of the pulse decreases. At large angles of incidence ($\alpha = 79.5°$ and $82.5°$), the positive part of the pulse completely disappears and the photovoltage is generated in the form of a negative unipolar pulse. It should be added that when the direction of rotation of the electric field vector of the incident radiation changes (i.e., at left-hand circularly polarized laser beam) the polarities of the pulses shown in Figure 5 change to the opposite ones. Thus, the waveforms of the transverse photovoltage pulses at circular polarization strongly depend on the angle of incidence, which is not typical of the longitudinal photovoltage pulses at different polarizations (see Figure 3) and the transverse photovoltage pulses at linear polarization (see Figure 4).

The unusual dependence of the waveform of the transverse photovoltage pulses on the angle of incidence at circular polarization can be explained on the basis of the interaction of linear and circular photocurrents arising in the surface layer of the film as a result of the transformation of the incident circular polarization into elliptical polarization upon the refraction of light at the air/film interface.

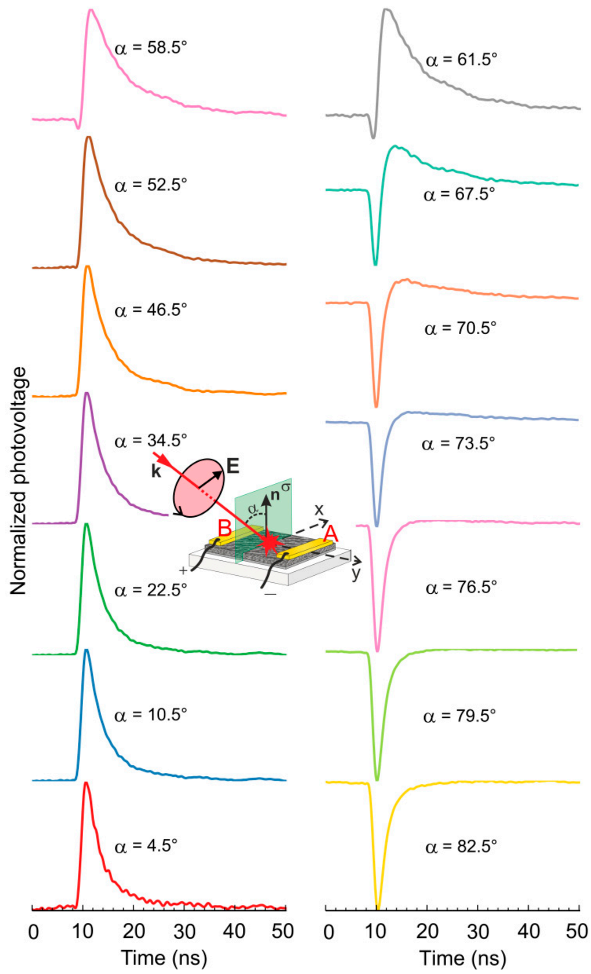


**Figure 5.** The waveforms of the transverse photovoltage pulses normalized to their extreme values for circularly polarized incident radiation, recorded for different angles of incidence $\alpha$. The inset shows the sketch of the experimental setup.

To determine the polarization of the refracted beam, one can use the complex Fresnel refractive indices $t_p$, $t_s$ for *p*- and *s*-polarizations, respectively, at the air/semitransparent film interface given in [66]:

$$t_p = \frac{2\hat{n}\cos\alpha}{\hat{n}^2\cos\alpha + \sqrt{\hat{n}^2 - \sin^2\alpha}}, t_s = \frac{2\cos\alpha}{\sqrt{\hat{n}^2 - \sin^2\alpha} + \cos\alpha}, \tag{5}$$

where $\hat{n} = n + i\kappa$ is the complex refractive index, $n$ is the real refractive index that determines the phase velocity ($n$ = 1.64), and $\kappa$ is the absorption coefficient ($\kappa$ = 2.14) that determines the attenuation of light in the film itself. From expression (5), the phase shift $\delta_t$ between the components of the refracted beam with *p*- and *s*-polarizations is determined by the formula:

$$\delta_t = -\delta_{tp} + \delta_{ts} + \delta_0, \tag{6}$$

where:

$$\delta_{tp} = \mathrm{Arg}(t_p) = \tan^{-1}\left(\frac{-\kappa^2\cos\alpha + \chi\cos\xi + n^2\cos\alpha}{\chi\sin\xi + 2\kappa n\cos\alpha}\right) - \tan^{-1}\left(\frac{n}{\kappa}\right), \tag{7}$$

$$\delta_{ts} = \mathrm{Arg}(t_s) = \tan^{-1}\left(\frac{(\cos\alpha + \chi\cos\xi)\csc\xi}{\chi}\right) - \frac{\pi}{2}, \tag{8}$$

$$\chi = \sqrt[4]{\left(-\sin^2\alpha - \kappa^2 + n^2\right)^2 + 4\kappa^2 n^2}, \quad (9)$$

$$\xi = \frac{1}{2\left(\frac{\pi}{2} - \tan^{-1}\left(\frac{-\sin^2\alpha - \kappa^2 + n^2}{2\kappa n}\right)\right)}, \quad (10)$$

$\delta_{tp}$, $\delta_{ts}$ are the phase shifts of the *p*- and *s*-beam components, respectively, resulting from refraction at the interface between two media with a complex refractive index, and $\delta_0$ is the initial phase shift between the *p*- and *s*-components before refraction. For the circular polarization of the incident radiation $\delta_0 = \pi/2$, where the signs "+" and "−" are the opposite of the sign of circular polarization.

It follows from Equation (5) that the amplitude values of the complex transmission coefficients $t_p$ and $t_s$ can be determined using:

$$|t_p| = \frac{2\cos\alpha\sqrt{\kappa^2 + n^2}}{\sqrt{\left(-\kappa^2\cos\alpha + \chi\cos\xi + n^2\cos\alpha\right)^2 + \left(2\kappa n\cos\alpha + \chi\sin\chi\right)^2}}, \quad (11)$$

$$|t_s| = \frac{2\cos\alpha}{\sqrt{\chi^2\sin^2\xi + \left(\cos\alpha + \chi\cos\xi\right)^2}}. \quad (12)$$

The amplitudes of the *p*- and *s*-components of the electric field vector of the refracted beam $\mathbf{E}^{(\mathbf{t})}$ describing the ellipse in the x″y coordinate system can be found using the equations:

$$T_{x''} = |t_p|E_p;\ T_y = |t_s|E_s, \quad (13)$$

respectively, where x″y is the coordinate plane perpendicular to the wave vector $\mathbf{k}_t$ of the refracted beam, axis x″ is in the plane of incidence σ, and the axis y is perpendicular to σ.

In this case, the equation of the polarization ellipse in the refracted beam depending on the ratio of the *p*- and *s*-components of the vector $\mathbf{E}^{(\mathbf{t})}$ and the phase shift $\delta_t$ can be written as follows:

$$\frac{(x'')^2}{{T_{x''}}^2} + \frac{y^2}{T_y^2} - \frac{2x''y\cos\delta_t}{T_{x''}T_y} = \sin^2\delta_t. \quad (14)$$

The polarization ellipses are characterized by the angle ψ between the semi-major axis *a* of the ellipse and the x″ axis lying in the incidence plane σ of radiation on the film (see Figure 6a,b right insets), as well as the degree of circular polarization $P_{cir} = \gamma 2ab/\left(a^2 + b^2\right)$ and degree of linear polarization $P_{lin} = \left(a^2 - b^2\right)/\left(a^2 + b^2\right)$, where *b* is the semi-minor axis of the ellipse, γ is the sign of circular polarization, and γ = 1 and γ = −1 denote the rotation of the electric field vector to the right and to the left, respectively.

Expression (14) makes it possible to calculate the angle ψ, as well as the length of the minor *b* and major *a* semiaxes of the refracted beam polarization ellipse using the following Equations:

$$\psi = \frac{1}{2}\tan^{-1}\left(\frac{2T_{x''}T_y\cos\delta_t}{{T_{x''}}^2 - {T_y}^2}\right), \quad (15)$$

$$a = \sqrt{\frac{1}{2}\left({T_{x''}}^2 + {T_y}^2 + \sqrt{{T_{x''}}^4 + {T_y}^4 + 2{T_{x''}}^2{T_y}^2\cos 2\delta_t}\right)}, \quad (16)$$

$$b = \sqrt{\frac{1}{2}\left({T_{x''}}^2 + {T_y}^2 - \sqrt{{T_{x''}}^4 + {T_y}^4 + 2{T_{x''}}^2{T_y}^2\cos 2\delta_t}\right)}. \quad (17)$$

Equations (16) and (17) were used to calculate $P_{cir}$ and $P_{lin}$. Figure 6a,b shows the calculated values of ψ, $P_{cir}$, and $P_{lin}$ for different angles α, for which the waveforms of the photovoltage pulses were recorded for circular and linear polarizations (Φ = −45°) of the incident radiation, respectively. It can be seen that when the incident beam is circularly polarized at large angles α, there is a significant change in the parameters ψ, $P_{cir}$, and $P_{lin}$ characterizing the polarization ellipse in the refracted beam. However, at α < 20°, the refracted beam remains virtually circularly polarized, i.e., at small angles of incidence, the polarizations of the incident and refracted beams virtually coincide. It should be added that at all $\alpha$, the signs of the circular polarization of the incident and refracted beams coincide, i.e., for both beams $\gamma = 1$.

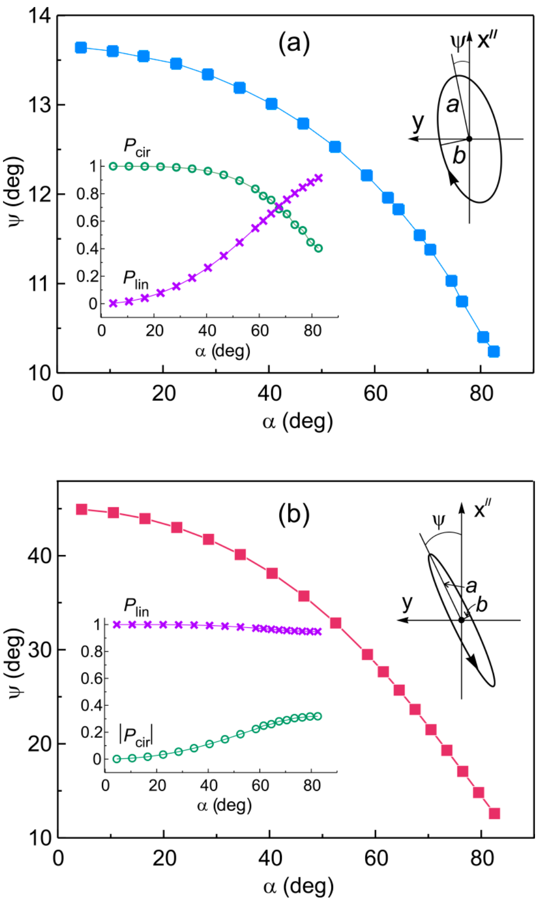


**Figure 6.** The angle ψ of the semi-major axis *a* of the refracted beam polarization ellipse relative to the plane of incidence σ, as well as the degrees of circular $P_{cir}$ and linear $P_{lin}$ polarizations of the refracted beam (insets) as a function of the angle of incidence α for (**a**) circularly and (**b**) linearly polarized (Φ = −45°) radiation incident on a thin CuSe/*t*-Se film (points are calculated values of ψ, $P_{cir}$ and $P_{lin}$ for angles α, for which photovoltage pulses were recorded, curves denote smoothing functions). The graphical insets show the corresponding calculated polarization ellipses of the refracted beam at α = 64.5° in the x″y coordinate system, where the x″ axis lies in the refraction plane coinciding with the plane of incidence σ and is perpendicular to the wave vector of the refracted beam.

It follows from Figure 6b that with linear polarization of the incident light at Φ = −45° the refracted beam is also elliptically polarized, but in this case $\gamma = -1$ (see upper inset). In addition, when changing α in the range of 0–85°, the modulus $P_{cir}$ of the refracted beam changes insignificantly from 0 to 0.32. At small angles α, the changes in the polarization state of the refracted beam are minimal.

It is known that the transverse photocurrent $j_y$ for elliptical excitation beam polarization consists of a CPC ($j_{y,cir}$) and an LPC ($j_{y,lin}$), i.e., $j_y = j_{y,cir} + j_{y,lin}$. According to [48] and taking into account [29], for positive angles of incidence, the transverse photocurrent amplitude in the CuSe/Se film structure for elliptical beam polarization can be represented as follows:

$$j_y = A_{cir} P_{cir} - A_{lin} P_{lin} \sin 2\psi, \tag{18}$$

where $A_{cir}$ and $A_{lin}$ are the positive coefficients of the circular and linear photocurrents at a given α, respectively. Taking into account Equation (18) and in accordance with the results of [37], the waveforms of the transverse photovoltage pulses $U_y(t, \alpha)$ can be written as follows:

$$U_y(t, \alpha) = B_{cir}(\alpha) P_{cir} f_{cir}(t) - B_{lin}(\alpha) P_{lin} \sin 2\psi \, f_{lin}(t), \tag{19}$$

where $B_{cir}(\alpha)$, $B_{lin}(\alpha)$ are positive coefficients (for positive $\alpha$) depending on $\alpha$ and characterizing the circular and linear contributions, respectively, and $f_{cir}(t)$ and $f_{lin}(t)$ are the transverse photovoltage waveforms normalized to the maximum values, recorded at angles $\alpha$ close to zero for circular and linear polarizations, respectively. Equation (19) allows one to approximate the waveforms of the photovoltage pulses, recorded at different $\alpha$, with two unknown parameters $B_{cir}(\alpha)$ and $B_{lin}(\alpha)$. For example, Figure 7 shows the approximations of the waveforms for four of the recorded pulses at different $\alpha$. It can be seen that the obtained approximating curves satisfactorily describe the experiment. It should be noted that if the waveforms $f_{cir}(t)$ and $f_{lin}(t)$ coincide with each other, the generation of bipolar pulses is impossible, and the duration of unipolar pulses of the resulting photocurrent, defined by Equation (19), does not depend on the angle of incidence.

Figure 8 shows the dependences of the calculated coefficients $B_{cir}$ and $B_{lin}$ on $\alpha$. It follows from the figure that both coefficients $B_{cir}$ and $B_{lin}$ approach zero at small and also at grazing angles of incidence. However, the dependences of $B_{cir}$ and $B_{lin}$ on $\alpha$ differ significantly from each other. It can be seen that the dependences of $B_{cir}$ and $B_{lin}$ acquire their extreme values at $\alpha = 54°$ and $\alpha = 62°$, respectively. The coefficient $B_{lin}$ prevails over $B_{cir}$ for the entire range of the incident angle change and the ratio $B_{lin}/B_{cir}$ increases monotonically with increasing $\alpha$.

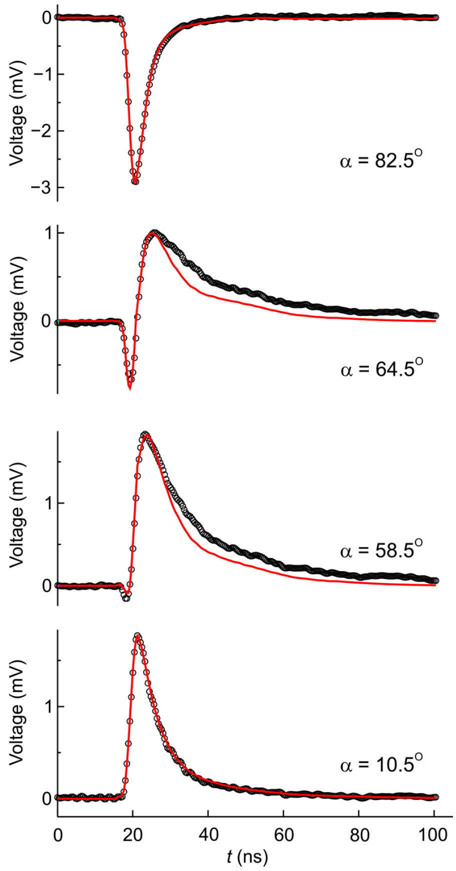


**Figure 7.** The oscillograms of the photovoltage pulses arising in a thin CuSe/*t*-Se film with circular polarization of exciting radiation and angles of incidence $\alpha$ = 10.5, 58.5, 64.5, and 82.5° (black circles), and their approximations shown by red lines according to Equation (19).

It follows from Figure 6b that with linear polarization ($\Phi = -45°$) of the incident beam, the refracted beam becomes elliptically polarized at a negative polarization sign ($\gamma = -1$). This means that both terms on the right side of Equation (19) remain negative for any positive angle of incidence. In addition, when changing $\alpha$ in the range of 0−85°, the parameters $P_{cir}$ and $P_{lin}$ of the refracted beam do not change significantly. Taking into account Equation (19), this leads to a weak dependence of the waveform of the photovoltage pulse on the angle $\alpha$ for linearly polarized laser pumping. It should be noted that the transverse photocurrent arising in the medium due to the PDE or CPGE also consists of the circular and linear contributions. Therefore, the temporal profile of the transverse photocurrent pulses of the PDE or CPGE generated in the nonlinear optical medium when pumped by short laser pulses of circular polarization can also depend in a complex way on the angle at which the light falls on the surface of the absorbing medium.

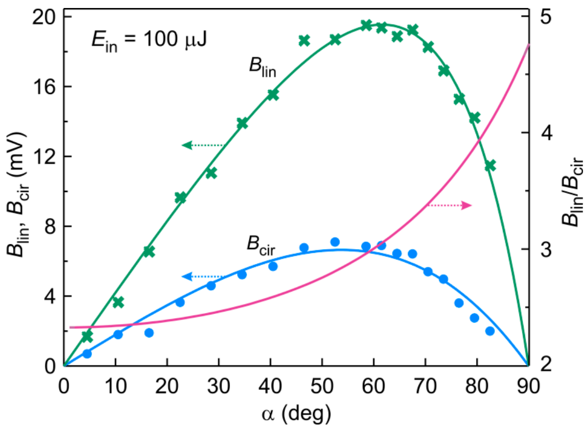


**Figure 8.** The coefficients $B_{\text{lin}}$ (green crosses), $B_{\text{cir}}$ (blue dots) as a function of the angle of incidence $\alpha$, which characterize the linear and circular contributions to the transverse photovoltage pulses, calculated from the experimental data (the green and blue curves represent the corresponding approximations by the equations $B_{\text{lin}} = 55.98 \sin 2\alpha/(1.15\cos\alpha + 1)^2$, $B_{\text{cir}} = 11.75 \sin 2\alpha\ /(0.5\cos\alpha + 1)^2$, respectively), and calculated dependence of the ratio $B_{\text{lin}}/B_{\text{cir}}$ on $\alpha$ (pink curve).

Good agreement between the experimental data and the calculated dependences confirms that the angular dependence of the waveforms of transverse photocurrent pulses in a thin CuSe/Se film under circularly polarized femtosecond laser pumping originates from the transformation of circular polarization into elliptical polarization upon refraction of light in a semitransparent CuSe/Se film and the interaction of LPC and CPC having different relaxation times in the film structure. As mentioned above, despite the large number of publications on the topic of generation of polarization-sensitive transverse photocurrent in various materials, arising by various mechanisms, such a phenomenon has not been observed before. It is possible that this is due to the fact that in many studies of the transverse photocurrent, cw laser radiation or nanosecond laser radiation has been used (see, for example, [33,67–69]).

The results obtained in this work can be used in various applications in optoelectronics. For example, the experimental setup presented in the inset to Figure 5 can be used for the fast direct detection of the circular polarization state of light. If at angles of incidence $0 < \alpha < 58.5°$ (for example, at $\alpha = 45°$) the photocurrent pulses generated in a CuSe/*t*-Se thin film have a positive polarity, then this means that the incident radiation is right-hand polarized (looking towards the light source). If, under the same experimental conditions, the photocurrent pulses have a negative polarity, then the incident radiation is left-hand polarized. This method of determining the state of circular polarization does not require the use of optical elements. Further, it is obvious that this photovoltaic property of a CuSe/Se thin film can be used to determine the fast and slow axes of a quarter-wave plate without using a reference quarter-wave plate and an optical light polarization.

## 4. Conclusions

In thin semitransparent CuSe/*t*-Se films synthesized by vacuum thermal deposition, the generation of nanosecond photocurrent pulses is studied as a function of the angle of incidence and polarization of exciting femtosecond laser pulses at 795 nm. It has been established that the dependences of the longitudinal and transverse photocurrents on the angle of incidence are described by odd relationships, which are characteristic of the SPGE nonlinear optical phenomenon. The relationships found for the longitudinal and transverse photocurrents as a function of pump polarization are also in agreement with the mechanism of photocurrent generation due to the SPGE. It is shown that the pulse durations of the longitudinal photocurrent for linear and circular polarizations, as well as the transverse photocurrent for linear polarization, are virtually independent of the incidence angle. However, the waveforms of the transverse photocurrent pulses at circular polarization with a given direction of rotation of the electric field vector of the incident radiation at a fixed sign of the angle of incidence strongly depend on the angle of incidence. At small and large angles of incidence, unipolar pulses of opposite polarity are generated, and in the intermediate range of incidence angles ($58.5 \leq \alpha \leq 76.5°$), bipolar photocurrent pulses are excited, smoothly transforming into unipolar pulses of opposite polarity at the boundaries of this interval. The obtained features of the waveform of the transverse photocurrent pulses at circular polarization of the incident radiation are due to the following: (i) the transformation of the circular polarization of the incident radiation into an elliptical one (without changing the sign of the circular polarization) upon the refraction of light at the air/semitransparent film interface and the appearance of a linear component of the photocurrent in the film structure, depending on the angle of incidence; (ii) the interaction of multidirectional linear and circular components of the photocurrent, which have different relaxation times and strongly depend on the angle of incidence.

The relationships found for the influence of the incidence angle on the waveform of pulses of longitudinal and transverse photocurrents that arise in the CuSe/*t*-Se film structure under polarized pulsed pumping due to the SPGE can be found in various materials in which the PSPC is excited by the PDE or by the CPGE.

The results obtained in this work can be used in optoelectronics, in particular, to create a high-speed detector capable of distinguishing left-handed and right-handed polarized light, as well as in the development of a technique that allows one to quickly determine the fast and slow axes of quarter-wave plates.

**Supplementary Materials:** The following supporting information can be downloaded at: https://www.mdpi.com/article/10.3390/app12146869/s1, Figure S1: X-ray diffractogram of the CuSe/*t*-Se nanocomposite film and diffraction patterns of CuSe (PDF 00-034-0171) and *t*-Se (PDF 00-042-1425) powders. A copper-based X-ray tube generating radiation at a wavelength of 0.1541 nm was used; Figure S2: Raman spectrum of the CuSe/*t*-Se nanocomposite film (black line). The red line represents the fitting of the combined Gaussian profiles at (blue line) 232 and (purple line) 237 cm$^{-1}$ corresponding to the *t*-Se and (green line) 262 cm$^{-1}$ to the CuSe nanocrystallites Raman resonances. A He-Ne laser radiation at a wavelength of 632.8 nm as excitation pumping was used; Figure S3: Scanning electron microscope image of the CuSe/*t*-Se semitransparent thin film surface; Figure S4: The optical transmittance spectrum of the CuSe/*t*-Se nanocomposite.

**Author Contributions:** Conceptualization, A.E.F. and G.M.M.; methodology, A.E.F., V.Y.K. and G.M.M.; validation, A.E.F., T.N.M., K.G.M. and G.M.M.; investigation, A.E.F., T.N.M., V.Y.K., K.G.M. and G.M.M.; resources, V.Y.K. and G.M.M.; writing—original draft preparation, A.E.F. and G.M.M.; writing—review and editing, all authors; supervision, G.M.M.; project administration, G.M.M. All authors have read and agreed to the published version of the manuscript.

**Funding:** This work was supported by the Ministry of Education and Science of the Russian Federation (state registration number 1021032422167-7-1.3.2) and the Academy of Finland (Grant Nos. 323053, 340115).

**Institutional Review Board Statement:** Not applicable.

**Informed Consent Statement:** Not applicable.

**Data Availability Statement:** Not applicable.

**Acknowledgments:** The authors are grateful to Y.P. Svirko for discussing the results obtained. This study was performed using equipment of the Shared Use Center "Center of Physical and Physicochemical Methods of Analysis and Study of the Properties and Surface Characteristics of Nanostructures, Materials, and Products" UdmFRC UB RAS.

**Conflicts of Interest:** The authors declare no conflict of interest.

## Nomenclature

| Symbol | |
|---|---|
| $\alpha$ | Angle of incidence |
| Se | Selenium |
| Cu | Copper |
| $t$-Se | Trigonal selenium |
| $E_{in}$ | Laser pulse energy |
| $R_{in}$ | Input impedance of the oscilloscope |
| $j_x$ | Longitudinal photocurrent |
| $j_y$ | Transverse photocurrent |
| $U_x$ | Extreme values of the voltage pulses at the experimental geometry when the measuring electrodes were placed perpendicular to the plane of incidence |
| $U_y$ | Extreme values of the voltage pulses at the experimental geometry when the measuring electrodes were placed parallel to the plane of incidence |
| $t$ | Time |
| $\eta_x$ | Efficiency of converting light into longitudinal photocurrent |
| $\eta_y$ | Efficiency of converting light into transverse photocurrent |
| $\Phi$ | Angle between the plane of polarization and the radiation incidence plane on the film |
| $\sigma$ | Radiation incidence plane on the film |
| $\mathbf{n}$ | Normal to the film surface |
| $\mathbf{A}$ | Measuring electrode |
| $\mathbf{B}$ | Measuring electrode |
| $\mathbf{k}$ | The wave vector of the optical field |
| $\mathbf{E}$ | Electric field vector of the incident radiation |
| $\mathbf{E}^{(\mathbf{t})}$ | Electric field vector of the refracted beam |
| x, y | Axes of the rectangular coordinate system |
| x′ | Axis, which lies in the σ plane and perpendicular to **k** |
| x″ | Axis, which lies in the refraction plane coinciding with the plane of incidence and perpendicular to the wave vector of the refracted beam |
| $t_p$ | Complex Fresnel refractive index for *p*-polarizations |
| $t_s$ | Complex Fresnel refractive index for *s*-polarizations |
| $\hat{n}$ | Complex refractive index |
| $n$ | Real refractive index that determines the phase velocity |
| $\kappa$ | Absorption coefficient |
| $\delta_t$ | Phase shift between the components of the refracted beam with *p*- and *s*-polarizations |
| $\delta_{tp}$ | Phase shift of the *p*-component of the beam, resulting from refraction at the interface between two media with a complex refractive index |
| $\delta_{ts}$ | Phase shift of the *s*-component of the beam, resulting from refraction at the interface between two media with a complex refractive index |
| $\delta_0$ | Initial phase shift between the *p*- and *s*-components before refraction |
| $a$ | Semi-major axis of the refracted beam polarization ellipse |
| $b$ | Semi-minor axis of the refracted beam polarization ellipse |
| $P_{cir}$ | Degree of circular polarization |
| $P_{lin}$ | Degree of linear polarization |
| $\psi$ | Angle between the semi-major axis of the refracted beam polarization ellipse and axis x″ |
| $\gamma$ | Sign of circular polarization |
| $U_y(t, \alpha)$ | Waveforms of the transverse photovoltage pulses |
| $A_{cir}$ | Positive coefficient of the circular photocurrent at a given α |
| $A_{lin}$ | Positive coefficient of the linear photocurrent at a given α |
| $B_{cir}$ | Positive coefficient (for positive α) depending on α and characterizing the circular contribution |
| $B_{lin}$ | Positive coefficient (for positive α) depending on α and characterizing the linear contribution |
| $f_{cir}(t)$ | Transverse photovoltage waveform normalized to its maximum value, recorded at angle α close to zero for circular polarizations |
| $f_{lin}(t)$ | Transverse photovoltage waveform normalized to its maximum values, recorded at angle α close to zero for linear polarizations |

**Abbreviations**

| | |
|---|---|
| PSPC | Polarization sensitive photocurrent |
| CPC | Circular photocurrent |
| LPC | Linear photocurrent |
| CPGE | Circular photogalvanic effect |
| PGE | Photogalvanic effect |
| PDE | Photon drag effect |
| SEM | Scanning electron microscope |
| FWHM | Full width at half maximum |

## References


1. Wang, J.; Zhou, Y.J.; Xiang, D.; Ng, S.J.; Watanabe, K.; Taniguchi, T.; Eda, G. Polarized light-emitting diodes based on anisotropic excitons in few-layer ReS2. *Adv. Mater.* **2020**, *32*, 2001890. [CrossRef] [PubMed]
2. Wang, X.; Wang, Q.; Zhang, X.; Miao, J.; Cheng, J.; He, T.; Li, Y.; Tang, Z.; Chen, R. Circularly polarized light source from self-assembled hybrid nanoarchitecture. *Adv. Opt. Mater.* **2022**, *2022*, 2200761. [CrossRef]
3. Seo, I.C.; Lim, Y.; An, S.C.; Woo, B.H.; Kim, S.; Son, J.G.; Yoo, S.; Park, Q.H.; Kim, J.Y.; Jun, Y.C. Circularly polarized emission from organic-inorganic hybrid perovskites via chiral fano resonances. *ACS Nano* **2021**, *15*, 13781–13793. [CrossRef] [PubMed]
4. Ivchenko, E.L. *Optical Spectroscopy of Semiconductor Nanostructures*; Springer: Berlin/Heidelberg, Germany, 2004.
5. Gurevich, V.L.; Laiho, R. Photomagnetism of metals. First observation of dependence on polarization of light. *Phys. Solid State* **2000**, *42*, 1807–1812. [CrossRef]
6. Singh, A.; Li, X.; Protasenko, V.; Galantai, G.; Kuno, M.; Xing, H.; Jena, D. Polarization-sensitive nanowire photodetectors based on solution-synthesized CdSe quantum-wire solids. *Nano Lett.* **2007**, *7*, 2999–3006. [CrossRef] [PubMed]
7. Luo, Y.; Hu, Y.; Xie, Y. Highly polarization-sensitive, visible-blind and self-powered ultraviolet photodetection based on two-dimensional wide bandgap semiconductors: A theoretical prediction. *J. Mater. Chem. A* **2019**, *7*, 27503–27513. [CrossRef]
8. Zhao, Q.; Gao, F.; Chen, H.; Gao, W.; Xia, M.; Pan, Y.; Shi, H.; Su, S.; Fang, X.; Li, J. High performance polarization-sensitive self-powered imaging photodetectors based on a p-Te/n-MoSe2 van der Waals heterojunction with strong interlayer transition. *Mater. Horiz.* **2021**, *8*, 3113–3123. [CrossRef]
9. Qian, L.; Zhao, J.; Xie, Y. Enhanced photogalvanic effect in the two-dimensional MgCl2/ZnBr2 vertical heterojunction by inhomogenous tensile stress. *Front. Phys.* **2022**, *17*, 13502. [CrossRef]
10. Karch, J.; Olbrich, P.; Schmalzbauer, M.; Zoth, C.; Brinsteiner, C.; Fehrenbacher, M.; Wurstbauer, U.; Glazov, M.M.; Tarasenko, S.A.; Ivchenko, E.L.; et al. Dynamic Hall effect driven by circularly polarized light in a graphene layer. *Phys. Rev. Lett.* **2010**, *105*, 227402. [CrossRef]
11. Ganichev, S.D.; Ivchenko, E.L.; Prettl, W. Photogalvanic effects in quantum wells. *Phys. E Low-Dimens. Syst. Nanostruct.* **2002**, *14*, 166–171.
12. Pan, Y.; Wang, Q.Z.; Yeats, A.L.; Pillsbury, T.; Flanagan, T.C.; Richardella, A.; Zhang, H.; Awschalom, D.D.; Liu, C.X.; Samarth, N. Helicity dependent photocurrent in electrically gated (Bi1-x Sb x )2Te3 thin films. *Nat. Commun.* **2017**, *8*, 1037. [CrossRef]
13. Zhang, Z.; Zhang, R.; Liu, B.; Xie, Z.L.; Xiu, X.Q.; Han, P.; Lu, H.; Zheng, Y.D.; Chen, Y.H.; Tang, C.G.; et al. Circular photogalvanic effect at inter-band excitation in InN. *Solid State Commun.* **2008**, *145*, 159–162. [CrossRef]
14. Mikheev, G.M.; Kogai, V.Y.; Mikheev, K.G.; Mogileva, T.N.; Saushin, A.S.; Svirko, Y.P. Polarization-sensitive photoresponse of the CuSe/Se nanocomposite prepared by vacuum thermal deposition. *Mater. Today Commun.* **2019**, *21*, 100656. [CrossRef]
15. Hägele, D.; Oestreich, M.; Rühle, W.W.; Nestle, N.; Eberl, K. Spin transport in GaAs. *Appl. Phys. Lett.* **1998**, *73*, 1580–1582. [CrossRef]
16. Okada, K.N.; Ogawa, N.; Yoshimi, R.; Tsukazaki, A.; Takahashi, K.S.; Kawasaki, M.; Tokura, Y. Enhanced photogalvanic current in topological insulators via Fermi energy tuning. *Phys. Rev. B* **2016**, *93*, 081403(R). [CrossRef]
17. Yu, J.; Zhu, K.; Zeng, X.; Chen, L.; Chen, Y.; Liu, Y.; Yin, C.; Cheng, S.; Lai, Y.; Huang, J.; et al. Helicity-dependent photocurrent of the top and bottom Dirac surface states of epitaxial thin films of three-dimensional topological insulators Sb2Te3. *Phys. Rev. B* **2019**, *100*, 235108. [CrossRef]
18. Mikheev, G.M.; Styapshin, V.M. Nanographite analyzer of laser polarization. *Instrum. Exp. Tech.* **2012**, *55*, 85–89. [CrossRef]
19. Akbari, M.; Ishihara, T. Polarization dependence of transverse photo-induced voltage in gold thin film with random nanoholes. *Opt. Express* **2017**, *25*, 2143–2152. [CrossRef]
20. Roy, S.; Manna, S.; Mitra, C.; Pal, B. Photothermal Control of Helicity-Dependent Current in Epitaxial $Sb_2Te_2Se$ Topological Insulator Thin-Films at Ambient Temperature. *ACS Appl. Mater. Interfaces* **2022**, *14*, 9909–9916. [CrossRef]
21. Mirzaee, S.M.A.; Lebel, O.; Nunzi, J.-M. A simple unbiased hot-electron polarization-sensitive near- infrared photo-detector. *ACS Appl. Mater. Interfaces* **2018**, *10*, 11862–11871. [CrossRef]
22. Li, W.; Coppens, Z.J.; Besteiro, L.V.; Wang, W.; Govorov, A.O.; Valentine, J. Circularly polarized light detection with hot electrons in chiral plasmonic metamaterials. *Nat. Commun.* **2015**, *6*, 8379. [CrossRef]
23. Schulz, M.; Balzer, F.; Scheunemann, D.; Arteaga, O.; Lützen, A.; Meskers, S.C.J.; Schiek, M. Chiral excitonic organic photodiodes for direct detection of circular polarized light. *Adv. Funct. Mater.* **2019**, *29*, 1900684. [CrossRef]

24. Wang, L.; Xue, Y.; Cui, M.; Huang, Y.; Xu, H.; Qin, C.; Yang, J.; Dai, H.; Yuan, M. A chiral reduced-dimension perovskite for an efficient flexible circularly polarized light photodetector. *Angew. Chemie* **2020**, *132*, 6504–6512. [CrossRef]
25. Hao, J.; Lu, H.; Mao, L.; Chen, X.; Beard, M.C.; Blackburn, J.L. Direct detection of circularly polarized light using chiral copper chloride-carbon nanotube heterostructures. *ACS Nano* **2021**, *15*, 7608–7617. [CrossRef] [PubMed]
26. Belinicher, V.I.; Sturman, B.I. The photogalvanick effect in media lacking of a center of symmetry. *Sov. Phys. Uspekhi* **1980**, *23*, 199–223. [CrossRef]
27. Ganichev, S.D.; Prettl, W.J. Spin photocurrents in quantum wells. *Phys. Condens. Matter.* **2003**, *15*, R935–R983. [CrossRef]
28. Zhang, Y.; Cao, R.; Hu, Y.; Wang, Y.; Xie, Y. A promising polarization-sensitive ultraviolet photodetector based on the two-dimensional ZrNBr-ZrNCl lateral heterojunction with enhanced photoresponse: A theoretical prediction. *Appl. Surf. Sci.* **2021**, *560*, 149907. [CrossRef]
29. Ivchenko, E.L. Circular photogalvanic effect in nanostructures. *Physics-Uspekhi* **2002**, *45*, 1299–1303. [CrossRef]
30. Ivchenko, E.L.; Spivak, B. Circular photogalvanic effect and related effects in chiral carbon nanotubes. *Physica* **2003**, *17*, 376–379. [CrossRef]
31. Dhara, S.; Mele, E.J.; Agarwal, R. Voltage-tunable circular photogalvanic effect in silicon nanowires. *Science* **2015**, *349*, 726–729. [CrossRef]
32. Moayed, M.M.R.; Li, F.; Beck, P.; Schober, J.-C.; Klinke, C. Anisotropic circular photogalvanic effect in colloidal tin sulfide nanosheets. *Nanoscale* **2020**, *12*, 6256–6262. [CrossRef]
33. Hubmann, S.; Budkin, G.V.; Otteneder, M.; But, D.; Sacré, D.; Yahniuk, I.; Diendorfer, K.; Bel'kov, V.V.; Kozlov, D.A.; Mikhailov, N.N.; et al. Symmetry breaking and circular photogalvanic effect in epitaxial CdxHg1-xTe films. *Phys. Rev. Mater.* **2020**, *4*, 043607. [CrossRef]
34. Sun, X.; Adamo, G.; Eginligil, M.; Krishnamoorthy, H.N.S.; Zheludev, N.I.; Soci, C. Topological insulator metamaterial with giant circular photogalvanic effect. *Sci. Adv.* **2021**, *7*, eabe5748. [CrossRef] [PubMed]
35. Glazov, M.M.; Ganichev, S.D. High frequency electric field induced nonlinear effects in graphene. *Phys. Rep.* **2014**, *535*, 101–138. [CrossRef]
36. Mikheev, G.M.; Saushin, A.S.; Vanyukov, V.V.; Mikheev, K.G.; Svirko, Y.P. Femtosecond circular photon drag effect in the Ag/Pd nanocomposite. *Nanoscale Res. Lett.* **2017**, *12*, 39. [CrossRef] [PubMed]
37. Akbari, M.; Onoda, M.; Ishihara, T. Photo-induced voltage in nano-porous gold thin film. *Opt. Express* **2015**, *23*, 823–832. [CrossRef]
38. Khichar, V.; Sharma, S.C.; Hozhabri, N. New features in the surface plasmon induced photon drag effect in noble metal thin films. *J. Phys. Commun.* **2021**, *5*, 055005. [CrossRef]
39. Al'perovich, V.L.; Belinicher, V.I.; Novikov, V.N.; Terekhov, A.S. Surface photovoltaic effect in solids. Theory and experiment for interband transitions in gallium arsenide. *Sov. Phys. JETP* **1981**, *53*, 1201–1208.
40. Mikheev, G.M.; Saushin, A.S.; Styapshin, V.M.; Svirko, Y.P. Interplay of the photon drag and the surface photogalvanic effects in the metal-semiconductor nanocomposite. *Sci. Rep.* **2018**, *8*, 8644. [CrossRef]
41. Guo, B.; Xiao, Q.L.; Wang, S.H.; Zhang, H. 2D Layered materials: Synthesis, nonlinear optical properties, and device applications. *Laser Photonics Rev.* **2019**, *13*, 1800327. [CrossRef]
42. You, J.W.; Bongu, S.R.; Bao, Q.; Panoiu, N.C. Nonlinear optical properties and applications of 2D materials: Theoretical and experimental aspects. *Nanophotonics* **2018**, *8*, 63–97. [CrossRef]
43. Gibson, A.F.; Kimmitt, M.F.; Walker, A.C. Photon drag in germanium. *Appl. Phys. Lett.* **1970**, *17*, 75–77. [CrossRef]
44. Noginova, N.; Rono, V.; Bezares, F.J.; Caldwell, J.D. Plasmon drag effect in metal nanostructures. *New J. Phys.* **2013**, *15*, 113061. [CrossRef]
45. Mikheev, G.M.; Saushin, A.S.; Vanyukov, V.V. Helicity-dependent photocurrent in the resistive Ag/Pd films excited by IR laser radiation. *Quantum Electron.* **2015**, *45*, 635–639. [CrossRef]
46. Strait, J.H.; Holland, G.; Zhu, W.; Zhang, C.; Ilic, B.R.; Agrawal, A.; Pacifici, D.; Lezec, H.J. Revisiting the photon-drag effect in metal films. *Phys. Rev. Lett.* **2019**, *123*, 53903. [CrossRef] [PubMed]
47. Beregulin, E.V.; Valov, P.M.; Ryvkin, S.M.; Yaroshetskii, I.D.; Lisker, I.S.; Pukshanskii, A.L. Dragging of electrons by light in semimetals. *JETP Lett.* **1977**, *25*, 101–104.
48. Mikheev, G.M.; Fateev, A.E.; Kogai, V.Y.; Mogileva, T.N.; Vanyukov, V.V.; Svirko, Y.P. Helicity dependent temporal profile of the semiconductor thin film photoresponse. *Appl. Phys. Lett.* **2021**, *118*, 201105. [CrossRef]
49. Hirose, H.; Ito, N.; Kawaguchi, M.; Lau, Y.C.; Hayashi, M. Circular photogalvanic effect in Cu/Bi bilayers. *Appl. Phys. Lett.* **2018**, *113*, 222404. [CrossRef]
50. Saushin, A.S.; Mikheev, K.G.; Styapshin, V.M.; Mikheev, G.M. Direct measurement of the circular photocurrent in the Ag/Pd nanocomposites. *J. Nanophotonics* **2017**, *11*, 032508. [CrossRef]
51. Konchenkov, V.I.; Myachkova, A.A.; Zav'Yalov, D.V. Influence of a constant field on a circular photovoltaic effect in two-dimensional superlattices. *J. Phys. Conf. Ser.* **2020**, *1697*. [CrossRef]
52. Mirzaee, S.M.A.; Nunzi, J.-M. Searching for evidence of optical rectification: Optically induced nonlinear photovoltage in a capacitor configuration. *J. Opt. Soc. Am. B* **2019**, *36*, 53. [CrossRef]
53. Aleksandrovich, E.V.; Aleksandrovich, A.N.; Mikheev, G.M. Laser-induced modification of optical properties of glassy selenium films synthesized by vacuum thermal evaporation. *J. Non. Cryst. Solids* **2020**, *545*, 120249. [CrossRef]

54. Li, Q.; Qi, D.; Wang, X.; Shen, X.; Wang, R.; Tanaka, K. Femto- and nano-second laser-induced damages in chalcogenide glasses. *Jpn. J. Appl. Phys.* **2019**, *58*, 080911. [CrossRef]
55. Ambade, S.B.; Mane, R.S.; Kale, S.S.; Sonawane, S.H.; Shaikh, A.V.; Han, S.-H. Chemical synthesis of p-type nanocrystalline copper selenide thin films for heterojunction solar cells. *Appl. Surf. Sci.* **2006**, *253*, 2123–2126. [CrossRef]
56. Gosavi, S.R.; Deshpande, N.G.; Gudage, Y.G.; Sharma, R. Physical, optical and electrical properties of copper selenide (CuSe) thin films deposited by solution growth technique at room temperature. *J. Alloys Compd.* **2008**, *448*, 344–348. [CrossRef]
57. Hankare, P.P.; Khomane, A.S.; Chate, P.A.; Rathod, K.C.; Garadkar, K.M. Preparation of copper selenide thin films by simple chemical route at low temperature and their characterization. *J. Alloys Compd.* **2009**, *469*, 478–482. [CrossRef]
58. Yakuphanoglu, F.; Viswanathan, C. Electrical conductivity and single oscillator model properties of amorphous CuSe semiconductor thin film. *J. Non. Cryst. Solids* **2007**, *353*, 2934–2937. [CrossRef]
59. Gao, L.; Sun, J.T.; Lu, J.C.; Li, H.; Qian, K.; Zhang, S.; Zhang, Y.Y.; Qian, T.; Ding, H.; Lin, X.; et al. Epitaxial growth of honeycomb monolayer CuSe with Dirac nodal line fermions. *Adv. Mater.* **2018**, *30*, 1707055. [CrossRef]
60. Jadhav, C.D.; Rondiya, S.R.; Hambire, R.C.; Baviskar, D.R.; Deore, A.V.; Cross, R.W.; Dzade, N.Y.; Chavan, P.G. Highly efficient field emission properties of vertically aligned 2D CuSe nanosheets: An experimental and theoretical investigation. *J. Alloys Compd.* **2021**, *875*, 159987. [CrossRef]
61. Ho, S.M. Fabrication of Cu 4 SnS 4 Thin Films: A Review. *Eng. Technol. Appl. Sci. Res.* **2020**, *10*, 6161–6164. [CrossRef]
62. Shinde, M.S.; Ahirrao, P.B.; Patil, I.J.; Patil, R.S. Thickness dependent electrical and optical properties of nanocrystalline copper sulphide thin films grown by simple chemical route. *Indian J. Pure Appl. Phys.* **2012**, *50*, 657–660.
63. Ezenwa, I.A.; Okereke, N.A.; Okoli, L.N. Electrical properties of copper selenide thin film. *IPASJ Int. J. Electr. Eng.* **2013**, *1*, 1–4.
64. García, V.M.; Nair, M.T.S.; Nair, P.K.; Zingaro, R.A. Chemical deposition of bismuth selenide thin films using N,N-dimethylselenourea. *Semicond. Sci. Technol.* **1997**, *12*, 645–653. [CrossRef]
65. Mikheev, G.M.; Kogai, V.Y.; Mikheev, K.G.; Mogileva, T.N.; Saushin, A.S.; Svirko, Y.P. Interaction of the polarization-sensitive surface photocurrents in the semitransparent CuSe/Se film. *Opt. Express* **2021**, *29*, 2112–2123. [CrossRef]
66. Saushin, A.S.; Mikheev, G.M.; Vanyukov, V.V.; Svirko, Y.P. The surface photogalvanic and photon drag effects in Ag/Pd metal-semiconductor nanocomposite. *Nanomaterials* **2021**, *11*, 2827. [CrossRef] [PubMed]
67. Zonov, R.G.; Mikheev, G.M.; Obraztsov, A.N.; Svirko, Y.P. Circular photocurrent in the carbon nanowall film. *Opt. Lett.* **2020**, *45*, 2022–2025. [CrossRef]
68. Wang, S.; Zhang, H.; Zhang, J.; Li, S.; Luo, D.; Wang, J.; Jin, K.; Sun, J. Circular Photogalvanic Effect in Oxide Two-Dimensional Electron Gases. *Phys. Rev. Lett.* **2022**, *128*, 187401. [CrossRef]
69. Li, M.; Yu, J.; Cui, G.; Chen, Y.; Lai, Y.; Cheng, S.; He, K. Circular photogalvanic effect of surface states in the topological insulator Bi2(Te0.23Se0.77)3 nanowires grown by chemical vapor deposition. *J. Appl. Phys.* **2022**, *131*, 113902. [CrossRef]